Recent experimental studies of ion acceleration driven by intense laser radiation pressure – Parametric scan and energy scaling

S. Kar[1], K.F. Kakolee[1], B. Qiao[2], M. Cerchez[3], D. Doria[1], A. Macchi[4], P. McKenna[5], J. Osterlholz[3], K. Quinn[1], B. Ramakrishna[1], G. Sarri[1], O. Willi[3], X. Yuan[5], M. Zepf[1], M. Borghesi[1]

[1] *Centre for Plasma Physics, Queen's University Belfast, BT7 1NN, Belfast, UK*

[2] *Center for Energy Research,University of California San Diego, CA 92093-0417 USA*

[3] *Institut für Laser-und Plasmaphysik, Heinrich-Heine-Universit¨at, D¨usseldorf, Germany*

[4] *Dipartimento di Energetica, Università di Roma 1 'La Sapienza', Roma, Italy*

[5] *Department of Physics, University of Strathclyde, Glasgow, UK*

Abstract

Radiation Pressure Acceleration (RPA) mechanism is currently attracting a substantial amount of experimental and theoretical attention worldwide. Employing the Petawatt laser of the Rutherford Appleton Laboratory, UK, both the Hole-boring (HB) and Light sail (LS) regimes of RPA have been extensively explored by scanning over wide range of laser and target parameters. The dominant role of laser radiation pressure in such intense interaction conditions resulted in narrow band heavy ion spectra, where the ion energy scales with $(I\tau/\xi)^{1.5}$ [I, τ and ξ stand for laser intensity, pulse duration and target areal density respectively] - significantly faster than the competing 'Target Normal Sheath Acceleration' mechanism ($E \propto I^{0.5}$). The aftermath of RPA is observed in the late time (0.1 - 1 ns) evolution of collimated plasma jets ejected from the target rear surface, detected by ps time resolved transverse interferometry. Significant Improvement in spatial uniformity of the plasma jet density profile observed for circularly polarised laser compared to linear polarisation is a clear indicative of the role played by circular polarisation towards stability of the RPA.

1. Introduction:

Ion acceleration from solid targets irradiated by high-intensity pulses has been one of the most attractive areas of research in the last decade due to its widespread potential applications in science, technology and healthcare [1]. Although ions up to MeV energy were produced in 1960-1980s by using $C0_2$ lasers, the field emerged in the last decade with the discovery of MeV ions accelerated by the so-called Target Normal Sheath acceleration (TNSA) mechanism [2]. In this process, ions are driven by a strong sheath field established at the target (foils of the order of micron thickness) rear surface by the relativistic electrons produced during the laser interaction. As a result several tens of MeV ions were produced with a beam-like feature and exceptionally high laminarity, which intrigued wide range of potential applications across wide range of disciplines [1]. For instance, the beam properties enable to study evolution of superstrong electromagnetic field profiles during intense laser-plasma interaction, with unprecedented temporal and spatial resolution, by a technique called 'proton projection imaging' [3].

However, low particle density (of the order of 10^{12} /MeV/Sr), 30^{o}-50^{o} divergence, and 100% energy spread of the proton beam poses significant limitations for many of the envisioned applications mentioned above, for instance, treatment of deep seated tumours. On the other hand, ion beam driven by the ultrahigh radiation pressure (of the order of 100s of Gbar for 10^{21} W/cm^2 laser intensity) of intense lasers has been predicted to be a promising route for accelerating large numbers of ions quasi-monoenergetically to ''relativistic'' energies (GeV/nucleon range) [4,5] in a significantly more efficient manner compared to TNSA. Therefore Radiation pressure acceleration (RPA) mechanism is currently attracting a substantial amount of experimental [6,7] and theoretical [4,5,8] attention worldwide.

Employing the Petawatt lasers of the Rutherford Appleton Laboratory, UK, both the Hole-boring (HB) and Light-sail (LS) regimes of RPA have been extensively explored. When the target thickness is of the order of hole-boring velocity times the laser pulse duration, highly collimated plasma jets of near solid density are ejected from the foil, lasting up to ns after the laser interaction. By changing the linear polarisation of the laser to circular, improved homogeneity in the jet's spatial density profile is achieved which suggests more uniform and sustained radiation pressure drive on target ions. By decreasing the target areal density or increasing irradiance on the target, the LS regime of the RPA is accessed where relatively high flux (~ 10^{12} particles/MeV/Sr) of ions are accelerated up to 20 MeV/nucleon energies in a narrow energy bandwidth. The ion energy in this regime, obtained from the parametric scans, scales with $(I\tau/\xi)^{1.5}$ where I, τ and ξ stand for laser intensity, pulse duration and target areal density respectively. Theoretical estimation based on RPA mechanism and 2D particle-in-simulations are in agreement with the experimental data in terms of ion energy and narrow band spectral feature.

2. Experimental Setup:

The experiment was carried out using the VULCAN Nd:glass laser of the Rutherford Appleton Laboratory, U.K., operating in chirped pulse amplification (CPA) mode. The laser wavelength and full width at half maximum (FWHM) pulse duration are 1.053 μm and 750 fs respectively. The laser was focused down on the target at near normal incidence by using an *f*/3 off-axis parabola. In order to reduce the pre-pulses and to

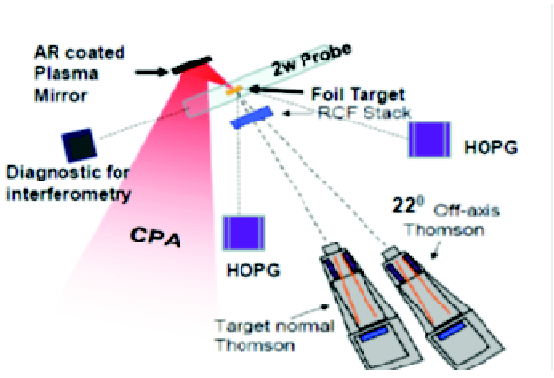

Fig 1: Schematic of the experimental setup.

suppress the intensity of amplified spontaneous emission, a plasma mirror was employed before the target. A schematic of the experimental setup is shown in the Fig. 1. A zero order quarter wave plate was used in the focusing beam, before the plasma mirror, in order to change the polarisation of the laser on the target. The intensity on the target was varied from 5×10^{19} W/cm^2 to 3×10^{20} W/cm^2 by increasing the laser spot size on the target, by translating the parabola along the focussing axis. Targets of various materials (Cu, Al, Au and CH) and thickness (10 μm down to 100 nm thickness) were used.

Two high resolutions Thompson Parabola Spectrometers were fielded in order to measure the ion spectra along the target normal direction and 22^0 off to the target normal. Hydrodynamic expansion of the plasma jets emerged from the target rear surface was characterised by employing transverse Nomarsky interferometer and shadowgraphy with high spatial (few microns) and temporal (ps) resolutions. The setup was designed to achieve two ps snapshots of the interaction at different times in a single shot.

3. Result and Discussions:

Basically in the RPA mechanism, ions are accelerated by directional momentum transfer from laser to target via the laser ponderomotive force, which acts as a snow-plow on the target front surface and launches a dense ion bunch into the target. In a cyclic fashion, the radiation pressure instantly pushes the electrons in the skin depth, which sets a strong accelerating field for ions to follow promptly the electrons. Consequently, the laser pulse bores through the target (hence called Hole-boring (HB) regime) where the ion front velocity (hole boring velocity) depends on the laser intensity (I) and target mass density (ρ). If the target thickness is less than the product of the laser pulse duration and hole boring velocity,

the ions will pile up at the target rear surface before the end of the laser pulse. As the thickness of the compressed layer become comparable or less than the evanescence length of the ponderomotive force, the whole layer is cyclically accelerated with high efficiency for the rest of the duration of the intense laser pulse. The latter scenario of whole foil acceleration is called light-sail (LS) regime. In this implementation employing ultrathin foils, ions are predicted to be accelerated to GeV/nucleon energy with next generation lasers, showing a coconlike deformation of ultrathin foils in 3D particle in cell simulation [9]. Although without reaching the dramatic effects at the currently achievable laser intensity, narrow bandwidth, peaked ion spectra are obtained in our experiment with energy reaching upto 20 MeV/nucleon - highest ion energy reported so far. However, by the time the RPA-LS become dominant at the moderate laser intensity of the order of 10^{20} W/cm^2 attained in current experiments, hot electron population created during the interaction allows the TNSA mechanism to grow in competition with RPA-LS. By varying laser and target parameters, we identified the transition from pure TNSA to TNSA-LS hybrid type ion acceleration in the experimental data. In the later situation an exponential ion spectra, marking the TNSA acceleration of the target rear contaminant ions has been observed being superseded towards higher energy side by a peaked ion spectral feature due to LS acceleration. Below we have summarised main results obtained from the experimental campaign, by systematically varying target (material and thickness) and laser (intensity and polarisation) parameters.

3.1 Sub-Mev ion jet by HB mechanism

The temporal evolution of the collimated plasma jets at the target rear side was observed from 150 ps to 1.1 ns, after the arrival of the CPA on the target. By comparing the jet

expansion velocity at late times, obtained from the analysis of interferograms, with hydrodynamic simulations, an estimation for velocity of ions attained by the HB mechanism is obtained. Fig. 2(a) shows the ion velocity obtained over several shots, taken at various laser and target parameters, plotted against a parameter 'Ω = target thickness/HB velocity'. The HB velocity is calculated from the expression, $c\sqrt{\Xi}/(1+\sqrt{\Xi})$, where $\Xi = I/\rho c^3$ and c is the speed of light in vacuum [8]. 'Ω' corresponds to the time required by the HB ions from the target front surface to reach the rear. As expected, because of collisional energy loss by the ions in the bulk of the target, the ion velocity falls gradually as Ω increases. The ion velocity attains maximum value when the incidence laser pulse duration is comparable to Ω. Lowering further the parameter Ω, by increasing the laser intensity, or, by decreasing the target density or thickness, the plasma jet start to lose their cohesion, forming filamentary features (see Fig. 2(c)). The loss of uniformity appears to be faster for linear polarisation of incident laser compared to circular polarisation, most likely due to significantly higher fast electron heating of the target for linear polarised laser interaction [4,5]. Detail analysis of the data is currently under progress. However, it is anticipated that the loss of cohesion of jets for 'Ω ~ incident laser pulse duration', is as a result of complete hole boring of target before the end of the incidence laser pulse. In fact, for significantly lower value of Ω, we could not able to observe a sustained jet formation, even for 100s of ps duration.

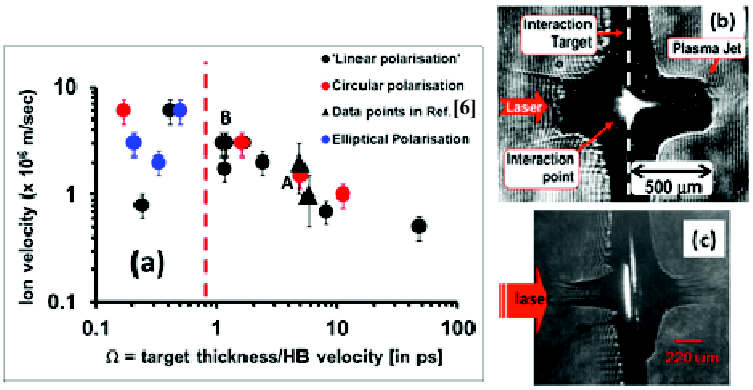

Fig 2. (a) Graph showing estimated ion velocity for different value of Ω, a parameter that depends on the laser and target parameters (as explained in the text). The red dotted line indicates the pulse duration of laser used in our experiment. **(b)** and **(c)** shows the interferograms correspond, respectively, to the data points 'A' and 'B' in (a).

3.2 LS-TNSA hybrid acceleration

In case of $\Omega \leq 1$, i.e. for very thin targets irradiated by high intensity, ion spectra along the target normal direction showed peaked feature towards higher energy side of the spectrum as shown in the Fig. 3(a). This is by contrast to the quasi-maxwellian spectra obtained for Ω > 1 (see Fig. 3(b) for instance) obtained typically.

Since for the ultra-thin targets, HB accelerated ions from the target front surface reach the target rear surface within a fraction of laser pulse duration (0.1 ps for the case shown in the Fig. 3(a)), the remaining duration of the CPA is spent in accelerating the ions in LS regime which has resulted in a peaked spectral feature in both the heavy ion and proton spectra. Ion energy attained by the LS mechanism scales with the ratio between laser intensity and target areal density, given by [4,5] $\beta_{LS} = \frac{(1+\psi)^2-1}{(1+\psi)^2+1}$, where $\psi = 2\pi \frac{Z}{A}\frac{m_e}{m_p}\frac{a_0^2 \tau_{LS}}{\zeta}$. Here $a_o = 0.85\sqrt{I\lambda^2/10^{18}\, W cm^{-2}\mu m^2}$ is dimensionless laser amplitude; λ is the laser wavelength, n_e and l are the electron density and thickness of the compressed layer. τ_{LS} is the duration of the laser pulse used for LS acceleration. *Z* and *A* are the atomic number and mass number of the target ions, and, m_e and m_p are the masses of an electron and proton respectively. Using the laser and target parameters for the case shown in the Fig. 3(a) in a simple numerical modeling based on the LS equation, we found that ion energy of 8 MeV/nucleon is expected by the LS mechanism, which agrees well with the experimental data (see the data point 'A' in the Fig. 4). Particle-in-cell simulation carried out for a scaled down laser and target

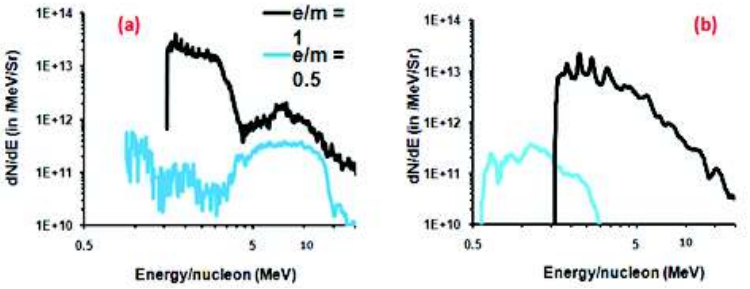

Fig 3. Experimental obtained spectra of two ion species for **(a)** thin (100 nm) and **(b)** thick (10 um) Cu targets irradiated at similar laser intensity and polarisation, which correspond to Ω ~ 0.1 and 10 respectively.

parameters also shows quasi-monoenergetic peak in ion spectra around 10 MeV/nucleon, which further substantiate the role of LS mechanism during the interaction.

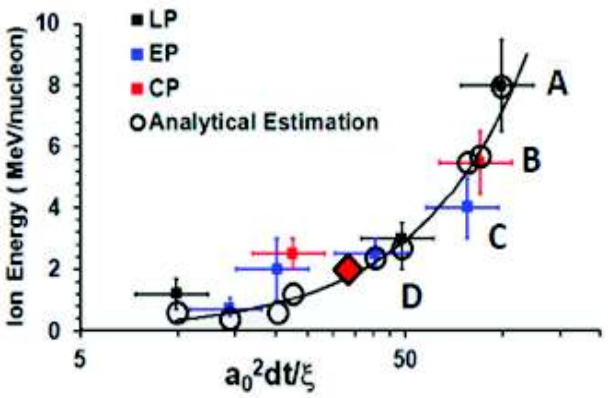

Fig 4: Graph showing the peak energy (/nucleon) of the ions (e/m=0.5) obtained experimentally for different laser and target parameters, plotted against the parameter $a_o^2\tau_{LS}/\zeta$. The red diamond with the black outer line represents the previously reported experimental data by Heing et. al.[7]. The experimental parameter set (intensity, target material, target thickness) for the data points marked as A, B, C and D are (3×10^{20} W/cm^2, Cu, 0.1µm), (1.25×10^{20} W/cm^2, Cu, 0.05µm), (2.2×10^{20} W/cm^2, Cu, 0.1µm), (6×10^{19} W/cm^2, Al, 0.1µm) respectively. The circles represent the results from simple numerical modeling based on the eq. (1). Data point 'A' corresponds to the case shown in the Fig. 3(a).

Finally, the scaling of RPA-LS acceleration regime has been obtained by a methodical scan over a range of target thickness, density, laser intensity and polarization. Fig 4 shows Ion energy scaling with the relevant scaling parameter $a_o^2\tau_{LS}/\zeta$. The data provide compelling experimental evidence for dominance of LS acceleration over TNSA. We can also see that, there is a good agreement between experimental data and RPA estimation for the other data points in the rising slope of the trend in the Fig. 4. The experimental data points shows that the ion energy scales with $(a_o^2\tau_{LS}/\zeta)^{1.5}$, which is significantly faster than the TNSA scaling, $E \propto a_o$.

4. Conclusion:

By contrast to the well-established TNSA mechanism, apparently RPA is a potential route for next generation, compact, laser driven ion accelerator due to its superior scaling in terms of ion energy and laser-ion conversion efficiency. Employing the Petawatt laser of the Rutherford Appleton Laboratory, UK, both HB and LS regimes of the RPA have been

explored by systematically scanning over a wide range of target and laser parameters. The data shows the transition from pure TNSA type ion acceleration from several micron thick targets to LS dominant LS-TNSA hybrid acceleration as decreasing the target thickness or increasing the laser intensity on the target. In the latter case, the interaction produced striking narrow band heavy ion spectra of energy up to 20 MeV/nucleon. Ion energy scaling with respect to target and laser parameters in the LS dominated regime is obtained from the data set which agrees with theory and simulation. The role of circular polarization of incident laser towards stable RPA acceleration is suggested by the sustained cohesion of the collimated plasma jets produced following the interaction.

References:

[1] M. Borghesi *et. al.*, Fusion Science and Technology, 49, 412 (2006) and the references therein.

[2] E. Clark et al., Phys. Rev. Lett., 84, 670 (2000); R. Snavely et al., Phys. Rev. Lett., 85, 2945 (2000)

[3] M. Borghesi et al., Phys. Plasmas, 9, 2214 (2002).

[4] A. Robinson et. al., New. J. Phys. 10, 013021 (2008); B. Qiao et. al., Phys. Rev. Lett. 102, 145002 (2009).

[5] A. Macchi et., al., Phys. Rev. Lett. 94, 165003 (2005); A. Macchi et. al, New J Phys., 12, 045013 (2010).

[6] S. Kar *et al*, Phys. Rev. Lett., 100, 225004 (2008).

[7] A. Heing *et. al.,* PRL 103, 245003 (2009).

[8] A P L Robinson, et. al., Plasma Phys. Control. Fusion 51, 024004 (2009).

[9] T. Esirkepov et. al., Phys. Rev. Lett., 92, 175003 (2004)